Nanotechnology

PAPER

# Dielectric-loading approach for extra electric field enhancement and spatially transferring plasmonic hot-spots

To cite this article: Mingjie Wan *et al* 2021 *Nanotechnology* **32** 035205



IOP Publishing Nanotechnology

Nanotechnology **32** (2021) 035205 (9pp) https://doi.org/10.1088/1361-6528/abaf7f

# Dielectric-loading approach for extra electric field enhancement and spatially transferring plasmonic hot-spots

**Mingjie Wan[1], Jingyu Wu[1], Jun Liu[1], Zhuo Chen[1], Ping Gu[1], Peng Zhan[1], Zhenlin Wang[1] and Sergey I Bozhevolnyi[2]**

[1] National Laboratory of Solid State Microstructures, School of Physics and Collaborative Innovation Center of Advanced Microstructures, Nanjing University, Nanjing 210093, People's Republic of China
[2] Centre for Nano Optics, University of Southern Denmark, Campusvej 55, Odense M DK-5230, Denmark

E-mail: zchen@nju.edu.cn and zhanpeng@nju.edu.cn

Received 25 April 2020, revised 11 July 2020
Accepted for publication 14 August 2020
Published 22 October 2020

**Abstract**

Plasmonic nanoantennas have been widely explored for boosting up light-matter interactions due to their ability of providing strongly confined and highly enhanced electric near fields, so called 'hot-spots'. Here, we propose a dielectric-loading approach for hot-spots engineering by coating the conventional plasmonic nanoantennas with a conformal high refractive index dielectric film and forming dielectric-loaded plasmonic nanoantennas. Compared to the conventional plasmonic nanoantennas, the corresponding dielectric-loaded ones that resonate at the same frequency are able to provide an extra enhancement in the local electric fields and meanwhile spatially transfer the hot spots to the dielectric surfaces. These findings have important implications for the design of optical nanoantennas with general applications in surface enhanced linear and nonlinear spectroscopies. As a demonstration application, we show that the maximum achievable fluorescence intensity in the dielectric-loaded plasmonic nanoantennas could be significantly larger than that in the conventional plasmonic nanoantennas.

Keywords: nanoantenna design, hot-spot engineering, extra fluorescence enhancement

(Some figures may appear in colour only in the online journal)

## 1. Introduction

Plasmons—coherent oscillations of free electrons in metals—have the ability to concentrate light into subwavelength volumes and enhance local electromagnetic field [1], which is essential for a diverse range of nanophotonics technologies and devices [2]. Thus far, simple geometries with sharp features (e.g. metal tips [3–5], triangles [6, 7] and cubes [8, 9]) that rely on lightning rod effect and more complex geometries with nanoscale gaps (e.g. bow-ties [10–13] and film-coupled metal nanoparticle system [14, 15]) that are based on near-field mode coupling have been most commonly utilized to create hot-spots. Although intense local fields have been produced in these rationally designed plasmonic nanoantennas, it is still challenging to achieve higher electric field enhancement, for example, by further narrowing the gap-width in the plasmonic dimers, because quantum mechanical effects such as nonlocality [16] and electron tunneling [17] could reduce the build-up of charges of opposite sign on the two sides of the gap, thereby reducing the maximum achievable field enhancement [18].

On the other hand, the strongest local fields of the hot-spots always locate at the metal surfaces. This would not cause any adverse impacts on the applications such as strong light-matter coupling [7, 10] and surface enhanced Raman scattering [19], because matters in these applications are allowed to be in direct contact with the metal surface. However, in the plasmon-enhanced fluorescence applications, if light emitters (e.g. quantum dots, dye molecules or ions) are placed too close to a metal, their fluorescence would be quenched rather than enhanced due to the energy transfer to dark

 

plasmonic modes in the metal [20–24]. To enhance the fluorescence as much as possible in the plasmonic nanoantennas, the emitters are forced to be placed at a non-zero optimal distance from the metal surface [23]. Since the plasmon-induced strongest local fields locate at the metal surfaces and their intensities decay exponetionally with the distance from the metal surfaces, such a non-zero emitter-metal distance makes the field enhancement that the emitters could sense is smaller than the maximum field enhancement that the plasmonic nanoantennas could provide. In other words, the hot-spots of the plasmonic nanoantennas are underutilized in the plasmon-enhanced fluorescence applications, and thus inevitably inhibiting the excitation efficiency of emitters (which is proportional to the field intensity at the position of emitters [23]).

In the past few years, the shell-isolated metal nanoparticles (SHINs) consisting of a metal core with a dielectric coating have been demonstrated as an efficient substrate for surface enhanced fluorescence [25–28]. Since the SHINs have a thickness-controllable dielectric shell acting as a built-in spacer, the requirement of the optimal emitter-metal distance could be easily fullfilled. It has been experimentally demonstrated that the best fluoresncece enhancement factor could be achieved in the SHINs when the shell is tuned to an optimal thickness [26]. It should be noted that in these previously reported SHINs, only silica with a relatively low refractive index ($n \approx 1.46$) has been employed as shell material [25–28]. For such a low refractive index coating, the field enhancement at the outside dielectric surface of the SHINs (which could be sensed by the emitters) is still lower than that at the inside metal surface [26]. Therefore, making the full utilization of the maximum field enhancement of the hot-spots to maximize the excitation efficiency of the emitters remains a challenge in the silica-coated SHINs.

Here, we present a dielectric-loading approach to engineer both the spatial position and maximum field intensity of the hot-spots. We demonstrate that by conformally coating a thin dielectric layer with a high refractive index onto the conventional plasmonic nanoantennas, hot-spots can be transferred to the outer dielectric surface of the reslutant dielectric-loaded plasmonic nanoantennas. The maximum achievable field enhancement of the transferred hot-spots in the dielectric-loaded plasmonic nanoantennas is found to increase with the shell refractive index, and in particular, it could exceed the maximum field enhancement achieved in the corresponding conventional plasmonic nanoantennas that resonate at the same frequency, as the shell refractive index is larger than a certain value. The ability to spatially transfer the hot-spots to the dielectric surface and provide an extra enhancement in the local electric fields makes the dielectric-loaded plasmonic nanoantennas suitable for applications such as surface enhanced linear and nonlinear spectroscopies. As a demonstration application, we show that compared to the conventional plasmonic nanoantennas, the dielectric-loaded ones could improve the fluorescence intensity by mainly maximizing the excitation efficiency of the emitters.

## 2. Results and discussion

### 2.1. Hot-spots engineering

Let us start by considering the simplest conventional plasmonic nanoantenna—a single spherical Au nanoparticle (AuNP) of radius $R$ embedded in a homogeneous medium (e.g. air, $n = 1.0$), as shown in the inset in figure 1(a). In this case, the radius of the AuNPs could be optimized to maximize the field enhancement for a given incident wavelength. Figure 1(a) shows the field enhancement factors calculated at the surface point $P$ corresponding to the incident electric field direction as functions of the radius $R$ and the incident wavelength $\lambda$, in which the calculations are performed using the three-dimensional finite element-method software COMSOL Multiphysics and the permittivity of Au is taken from the experimental data [29]. By plotting a vertical line in figure 1(a), which corresponds to a chosen wavelength, the optimal radius for the maximum field enhancement could be directly obtained at this particular wavelength. For example, for a typical incident wavelength of $\lambda = 633$ nm, when the radius of the AuNP is optimized to $R = 74$ nm, the field enhancement in the AuNPs could reach the maximum value of $\sim$27, as indicated by the point $I$ in the dashed line in figure 1(a).

To engineer the spatial position of the hot-spots, a dielectric-loading strategy that involves conformally coating plasmonic nanoantennas with a thin layer of high refractive index dielectrics (relative to the surrounding medium) is proposed. It is noted that high refractive index dielectric coating would increase the effective refractive index of the surrounding medium and induce a red-shift in the localized surface plasmon resonances (LSPRs) of the dielectric-loaded plasmonic nanoantennas [30]. Therefore, the conventional plasmonic nanoantennas need to be scaled down before dielectric coating to possibly counteract the red-shift effect. In that case, the dielectric-loaded and conventional plasmonic nanoantennas can both be optimized to resonate at the same wavelength to achieve a fair comparison.

According to this strategy, dielectric-loaded AuNPs are constructed by firstly reducing the size of the AuNP from its original optimal size $R = 74$ nm to, for example, $r = 50$ nm, and consequently coating a thin dielectric layer (inset in figure 1(b)). Since the electric fields distributed outside of the dielectric-loaded AuNPs could be sensed by the external matters, in the following discussions we mainly focus on the external field enhancement at the dielectric surface. When the radius of the core AuNP is fixed to $r = 50$ nm, two degrees of freedom, including the shell refractive index and shell thickness, could be optimized to maximize the external field enhancement at the given incident wavelength of $\lambda = 633$ nm. Figure 1(b) shows the electric field enhancement factors calculated at $\lambda = 633$ nm at the dielectric surface point $Q$ corresponding to the incident electric field direction in the dielectric-loaded AuNPs with a fixed $r = 50$ nm as functions of shell thickness ($t$) and shell refractive index ($n$). Contour lines with a value of 27, which represents the maximum field enhancement factor achieved in the conventional AuNPs (point $I$ in

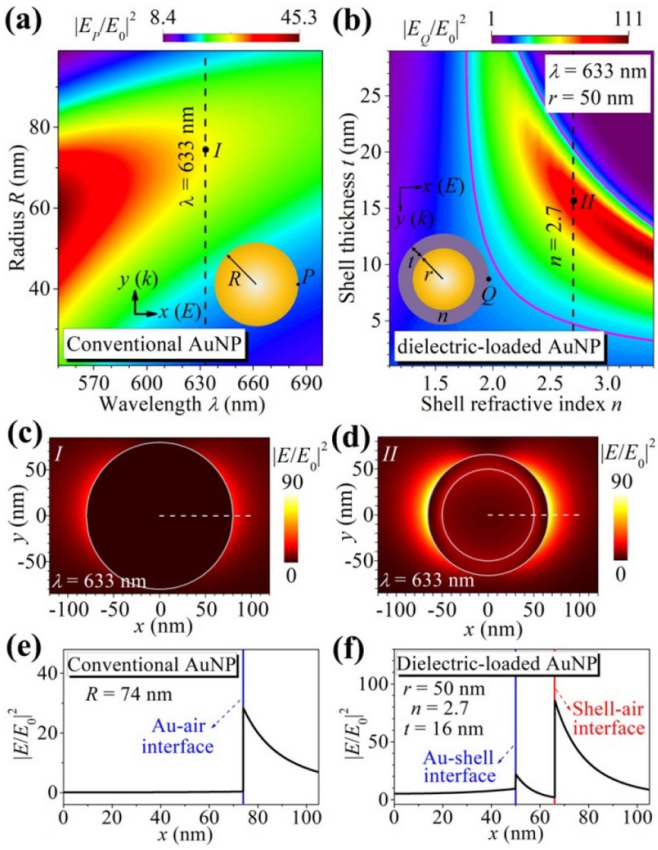


**Figure 1.** (a) The electric field intensity enhancement at the surface point $P$ of the AuNPs as functions of the radius and the incident wavelength. The vertical dashed line represents the incident wavelength of $\lambda = 633$ nm. (b) The electric field enhancement at the dielectric surface point $Q$ of the dielectric-loaded AuNPs with a fixed core radius $r = 50$ nm calculated for fixed wavelength $\lambda = 633$ nm as functions of the shell refractive index and the shell thickness. Solid lines are the contour lines with the value of 27. The vertical dashed line represents the shell refractive index of $n = 2.7$. Marked points *I* and *II* indicate the optimal case where the field enhancement is maximized. (c) and (d) The electric field distributions calculated at $\lambda = 633$ nm for the conventional and dielectric-loaded AuNPs with optimal parameters corresponding to the points *I* and *II*, respectively. (e) and (f) The electric field enhancement factors extracted along the central section lines in the conventional and dielectric-loaded AuNPs. Solid lines represent the interfaces.

figure 1(a)), are also plotted as red solid lines in figure 1(b). It is seen from figure 1(b) that as the shell refractive index and the shell thickness locate within the range enclosed by the contour lines, the dielectric-loaded AuNPs could produce larger external field enhancement than the conventional AuNPs. For example, for a shell refractive index of $n = 2.7$ (which is represented by a vertical dashed line in figure 1(b)), when the shell thickness is optimized to $t = 16$ nm, the external field enhancement at $\lambda = 633$ nm in the dielectric-loaded AuNPs can reach the maximum value of ~86, as indicated by the point *II* in figure 1(b).

The electric field distributions calculated at $\lambda = 633$ nm for the optimal conventional AuNP ($R = 74$ nm, corresponding to the point *I* in figure 1(a)) and the optimal dielectric-loaded AuNP ($r = 50$ nm, $n = 2.7$, $t = 16$ nm, corresponding to the point *II* in figure 1(b)) are shown in figures 1(c) and (d), respectively. As expected, for the conventional AuNP the strongest fields of the resonant hot-spots locate at the metal surface of the AuNP (figure 1(c)). After coating the AuNP with a thin dielectric layer, the resonant hot-spots are found to mostly distribute at the most outside surface of the dielectric-loaded AuNP (figure 1(d)), which directly validates that the dielectric-loading approach allows the strongest field of the hot-spots to be transferred from the metal surface to the dielectric surface.

Furthermore, the field enhancement factors extracted along the central section lines in the two optimal nanoantennas are plotted in figures 1(e) and (f), respectively. Associated with the excitation of the LSPR, electric fields are found to be enhanced at $x = R = 74$ nm in the conventional AuNP (as indicated by a blue vertical line in figure 1(e), which represents the Au-air interface) and $x = r = 50$ nm in the dielectric-loaded AuNP (as indicated by a blue vertical line in figure 1(f), which represents the Au-shell interface). It should be noted that compared to the conventional AuNPs, there is an additional interface between the high refractive index shell and the low refractive index surrounding medium (shell-air interface) in the dielectric-loaded ones. Due to the continuity boundary condition of the normal component of the electric displacement vector at the interface between two different materials [31], electric fields that decay away from the metal surface are expected to be abruptly enhanced at the shell-air interface in the dielectric-loaded AuNPs. As indicated by a red vertical line in figure 1(f), electric fields at $x = r + t = 66$ nm (corresponding to the dielectric surface of the dielectric-loaded AuNP) are indeed enhanced with a factor of ~86, which exceeds the maximum field enhancement factor of ~27 achieved in the optimal conventional AuNP. Therefore, in addition to the ability to spatially transfer the hot-spots from the metal surface to the dielectric surface, the dielectric-loading approach could also provide an extra enhancement in the local electric fields.

In practice, the dielectric materials that are suitable for acting as the shells of the dielectric-loaded plasmonic nanoantennas should be considered. Fortunately, dielectrics such as silica ($SiO_2$, $n \approx 1.46$) [25–28], alumina ($Al_2O_3$, $n \approx 1.8$) [32], zirconium dioxide ($ZrO_2$, $n \approx 2.1$) [33], zinc sulfide (ZnS, $n \approx 2.2$) [34], cerium oxide ($CeO_2$, $n \approx 2.3$) [35] and titanium dioxide ($TiO_2$, $n \approx 2.7$–$2.8$) [36] have been reported to be able to form a conformal shell around the noble metal NPs with a tunable shell thickness. Also, it is noted that in the above demonstration, to construct the dielectric-loaded plasmonic nanoantennas, the radius of the AuNP is, to some degree, reduced arbitrarily from $R = 74$ nm to $r = 50$ nm. Actually, the coating dielectric materials, i.e. the shell refractive index, could be firstly selected, and then the radius of the core AuNP and the shell thickness are simultaneously varied to maximize the external field enhancement in the dielectric-loaded AuNPs for a given incident wavelength

Figure 2(a) shows the electric field enhancement factors calculated at $\lambda = 633$ nm at the surface point $Q$ in the $TiO_2$-loaded AuNPs (with a fixed shell refractive index of $n = 2.7$) as functions of core radius ($r$) and the shell thickness ($t$). As

indicated by the marked point *III* in figure 2(a), when the core radius and the shell thickness are optimized to $r = 36$ nm and $t = 17$ nm, the $TiO_2$-loaded AuNPs could produce the external field enhancement factor as high as ∼112 at $\lambda = 633$ nm, which is 4 times larger than the maximum achievable field enhancement factor of ∼27 in the optimal conventional AuNP (point *I* in figure 1(a)). For direct comparison, the external field enhancement factors at $\lambda = 633$ nm in the $SiO_2$-loaded AuNPs (with a fixed shell refractive index of $n = 1.46$) are also plotted in figure 2(b) as functions of $r$ and $t$. The external field enhancement in the $SiO_2$-loaded AuNPs is found to monotonically decrease with increasing the shell thickness. As indicated by the marked point *IV* in figure 2(b), the external field enhancement reaches the maximum value of ∼27 at $r = 74$ nm and $t = 0$ nm, which is identical to the optimal case of the conventional AuNPs (point *I* in figure 1(a)). This reveals that due to the low shell refractive index, the $SiO_2$-loaded AuNPs are unable to provide higher external field enhancement than the optimal conventional AuNP. Therefore, the shell refractive index plays a key role in the dielectric loading approach. The maximum achievable external field enhancement factors at $\lambda = 633$ nm in the dielectric-loaded AuNPs with different shell refractive indices (i.e. different coating dielectrics) are summarized in figure 2(c). Provided that the shell refractive index is larger than $n = 1.7$, the dielectric-loaded AuNPs could always outperform the optimized conventional Au NP in terms of field enhancement. It is also found that the dielectric-loaded AuNPs with higher shell refractive index can produce larger external field enhancement. Therefore, the $TiO_2$ ($n = 2.7$) is chosen as dielectric shell materials in the following discussions.

In the above demonstrations, the incident wavelength is fixed to $\lambda = 633$ nm. The proposed dielectric-loading approach could also work for other incident wavelengths. Figures 3(a) and (b) show the external field enhancement in the $TiO_2$-loaded AuNPs with different core radii and shell thicknesses calculated at $\lambda = 590$ nm and $\lambda = 690$ nm, respectively. For these two incident wavelengths, the radius of the conventional AuNPs could be varied to maximize the field enhancement. It could be found from figure 1(a) that when the radius is optimized to $R = 67$ nm for $\lambda = 590$ nm and $R = 82$ nm for $\lambda = 690$ nm, the field enhancement in the conventional AuNPs could reach the maximum values of ∼33 and ∼23. As indicated by the marked points *V* and *VI* in figures 3(a) and (b), when the geometry parameters are optimized to ($r = 30$ nm, $t = 10.7$ nm) for $\lambda = 590$ nm and ($r = 42$ nm, $t = 25$ nm) for $\lambda = 690$ nm, the $TiO_2$-loaded AuNPs could produce the external field enhancement factors of ∼150 and ∼79, which are 3–4 times larger than the maximum field enhancements achieved in the optimal conventional AuNPs at the respective wavelengths. The electric field distributions calculated for the $TiO_2$-loaded AuNPs with optimal parameters (corresponding to the points *V* and *VI* in figures 3(a) and (b)) at $\lambda = 590$ nm and $\lambda = 690$ nm further present that the resonant electric fields are mostly distributed outside the dielectric-loaded AuNPs (figures 3(c) and (d)), which again validate the ability of the dielectric-loading approach to spatially transfer the hot spots to the dielectric surfaces.

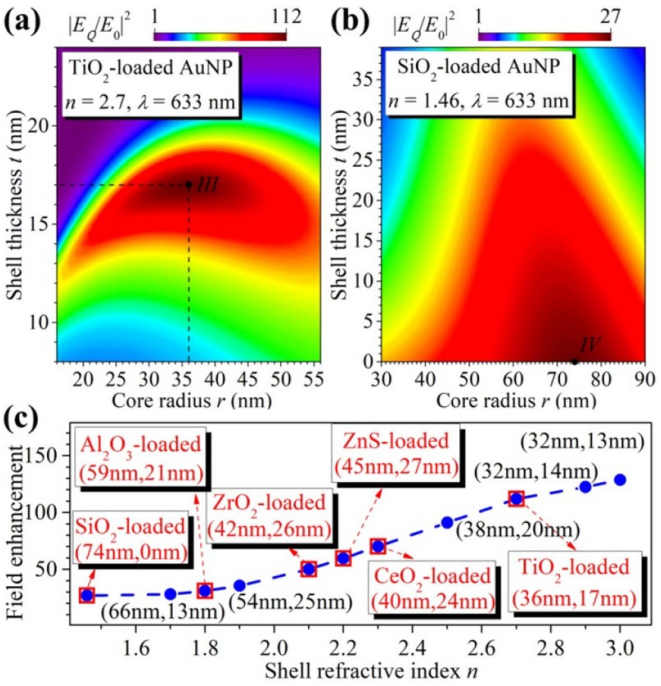


**Figure 2.** (a) and (b) The electric field enhancement at $\lambda = 633$ nm at the surface point $Q$ of the TiO2-loaded and the SiO2-loaded AuNPs as functions of the core radius and the shell thickness, respectively. Marked points *III* and *IV* indicate the optimal case where the external field enhancement is maximized. (c) The maximum achievable external field enhancement at $\lambda = 633$ nm in the dielectric-loaded AuNPs with different shell refractive indices. Hollow red squares represent some available dielectric materials.

### 2.2. Extra fluorescence enhancement

As a demonstration application, in what follows we show that compared to the conventional plasmonic nanoantennas the dielectric-loaded ones are able to provide an extra fluorescence enhancement. Here, we consider a single emitter (e.g. Nile blue dye molecule) interacting with the conventional and dielectric-loaded AuNPs, respectively. For weak excitation, the excitation and emission processes of an emitter could be treated independently because there is no coherence between the two processes [23]. To simulate the excitation process, the antennas are irradiated by a plane wave. Since the excitation rate of the molecule is proportional to the intensity of the local excitation field, its enhancement factor can then be written as

$$f_{exc} \equiv \gamma_{exc}/\gamma^0_{exc} = |\mathbf{n}_p.\mathbf{E}|^2/|\mathbf{n}_p.\mathbf{E}_0|^2 \tag{1}$$

where $\mathbf{n}_p$ is a unit vector pointing in direction of the molecule, $\mathbf{E}$ and $\mathbf{E}_0$ are the electric field with and without the antenna at the location of the molecule, respectively [23]. To simulate the emission process, the excited molecule is approximated as a classical dipole source. In the presence of the antenna, the normalized quantum yield of the molecule is given by

$$f_q \equiv q/q^0 = \frac{f_{rad}/q^0}{f_{rad} + f_{nrad} + (1 - q^0)/q^0} \tag{2}$$

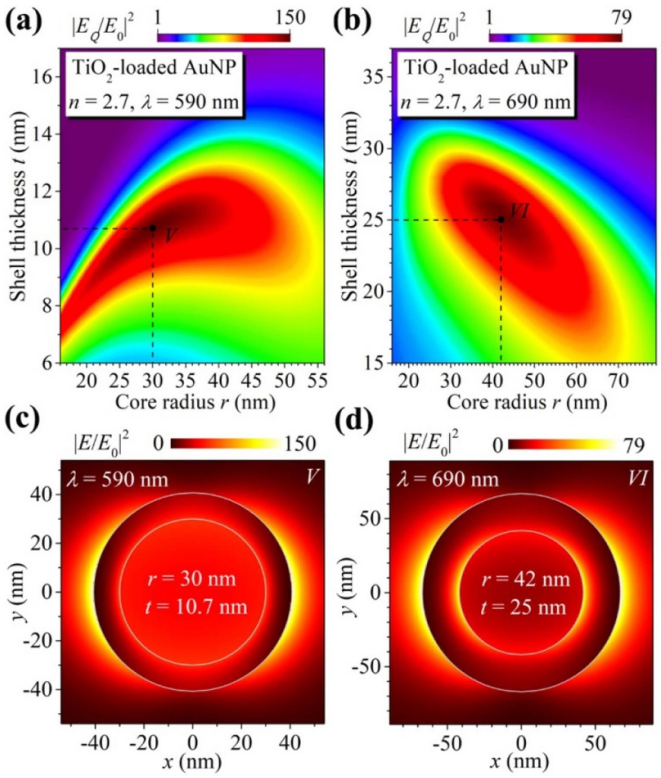


**Figure 3.** (a) and (b) The external electric field enhancement in the TiO2-loaded AuNPs as functions of the core radius and the shell thickness calculated for the incident wavelengths of $\lambda = 590$ nm and 690 nm, respectively. Marked points *V* and *VI* indicate the optimal case where the external field enhancement is maximized. (c) and (d) The electric field distributions calculated at $\lambda = 590$ nm and 690 nm for the $TiO_2$-loaded AuNPs with optimal parameters corresponding to the points *V* and *VI*, respectively.

where $q^0$ is the free-space intrinsic quantum yield of the molecule, and $f_{rad} \equiv \gamma_{rad}/\gamma^0_{rad}$ and $f_{nrad} \equiv \gamma_{nrad}/\gamma^0_{rad}$ are the normalized radiative and non-radiative decay rates, respectively [37–39]. The normalized energy-transfer rates in equation (2) could also be written as $f_{rad} \equiv P_{rad}/P_0$ and $f_{nrad} \equiv P_{nrad}/P_0$ with $P_{rad}$ being the power radiated into the far field by the dipole in the presence of the antenna, $P_{nrad}$ being the power dissipated in the metal part of the antenna due to ohmic loss, and $P_0$ being the power radiated by the same dipole in the absence of the antenna [40]. The normalized fluorescence rate is then obtained from the product of the normalized excitation rate and quantum yield, i.e. $f_{em} = \gamma_{em}/\gamma^0_{em} = f_{exc} f_q$.

For a single molecule placed near the conventional AuNPs (inset in figure 4(a)), its fluorescence enhancement is calculated and plotted in figure 4(a) as functions of the radius *R* and the molecule-Au separation distance *g*. In the calculations, the orientation of the molecule, the polarization of the excitation plane wave and the dipole source are along the axis connecting molecule and AuNP center. The wavelengths of the excitation plane wave and the dipole source are set to $\lambda_{exc} = 633$ nm and $\lambda_{em} = 663$ nm, which correspond to the peak absorption and emission of Nile blue molecules, respectively, such that the Stokes shift is empirically taken into account. The molecule is assumed to have unity intrinsic quantum yield $q^0 = 1$. As indicated by the point *I* in figure 4(a), when the molecule-Au separation distance and the radius of the conventional AuNP are optimized to $g = 11$ nm and $R = 78$ nm, the fluorescence enhancement could reach the maximum value of ∼11. The detailed energy-transfer rates $f_{exc}$, $f_q$ and $f_{em}$ of the molecule coupled to the conventional AuNP with a radius $R = 78$ nm for different molecule-Au separation distances are present in figure 4(b). It is found that with decreasing the molecule-Au separation distance, the excitation rate $f_{exc}$ increases due to the enhanced electric fields (blue curve in figure 4(b)), while the quantum yield $f_q$ decreases due to the increased non-radiative decay rate (dissipation in the metal) (green curve in figure 4(b)). As a result, the fluorescence enhancement $f_{em}$ can reach the maximum value when the balance between $f_{exc}$ and $f_q$ is achieved at an optimal molecule-Au separation distance $g = 11$ nm (red curve in figure 4(b)). Clearly, at this optimal separation distance $g = 11$ nm the excitation rate just reaches $f_{exc} \approx 14$, which is smaller than the maximum achievable rate of $f_{exc} \approx 27$ at $g = 0$ nm (corresponding to the Au surface), and thus revealing that the non-zero optimal emitter-metal separation distance prevents the emitter from fully utilizing the resonant hot-spot in the conventional plasmonic nanoantennas.

In the case of the dielectric-loaded AuNPs, the molecule is directly placed on the outer dielectric surface, as schematically shown in the inset in figure 4(c). The fluorescence enhancement factors of the single molecule coupled to the $SiO_2$-loaded AuNPs (with a fixed shell refractive index of $n = 1.46$) and the $TiO_2$-loaded AuNPs (with a fixed shell refractive index of $n = 2.7$) are plotted in figures 4(c) and (e), respectively, as functions of the core radius *r* and the coating thickness *t*. For the $SiO_2$-loaded AuNPs, when the geometrical parameters are optimized to $r = 68$ nm and $t = 17$ nm, the fluorescence intensity can reach a maximum enhancement factor of ∼19 (the point *II* in figure 4(c)). In particular, the maximum fluorescence enhancement achieved in the $TiO_2$-loaded AuNPs with optimal geometrical parameters of $r = 42$ nm and $t = 17$ nm is found to reach a factor as high as ∼57 (the point *III* in figure 4(e)), which is increased by about 5.2 times compared to the optimal case of the conventional AuNP, and thus validating that the dielectric-loading approach is able to further increase the maximum achievable fluorescence intensity.

To understand the origin of the extra fluorescence enhancement, the detailed energy-transfer rates of the molecule coupled to the $SiO_2$-loaded AuNPs with a fixed core radius of $r = 68$ nm (corresponding to the point *II* in figure 4(c)) and the $TiO_2$-loaded AuNPs with fixed $r = 42$ nm (corresponding to the point *III* in figure 4(e)) are plotted in figures 4(d) and (f), respectively, as a function of the coating thickness. The excitation rate and quantum yield in the $SiO_2$-loaded AuNPs (green and blue curves in figure 4(d)) are found to basically follow the same trend as those in the conventional AuNPs (green and blue curves in figure 4(b)). At the optimal $SiO_2$ coating thickness of $t = 17$ nm, the balance between $f_{exc}$ and $f_q$ is achieved. Compared to the optimal case of the conventional AuNPs, where the optimal molecule-Au separation distance is $g = 11$ nm, the 17 nm-thick $SiO_2$ shell provides a relatively larger molecule-Au separation distance. The normalized quantum yield of $f_q \approx 0.84$ achieved in the optimal case of

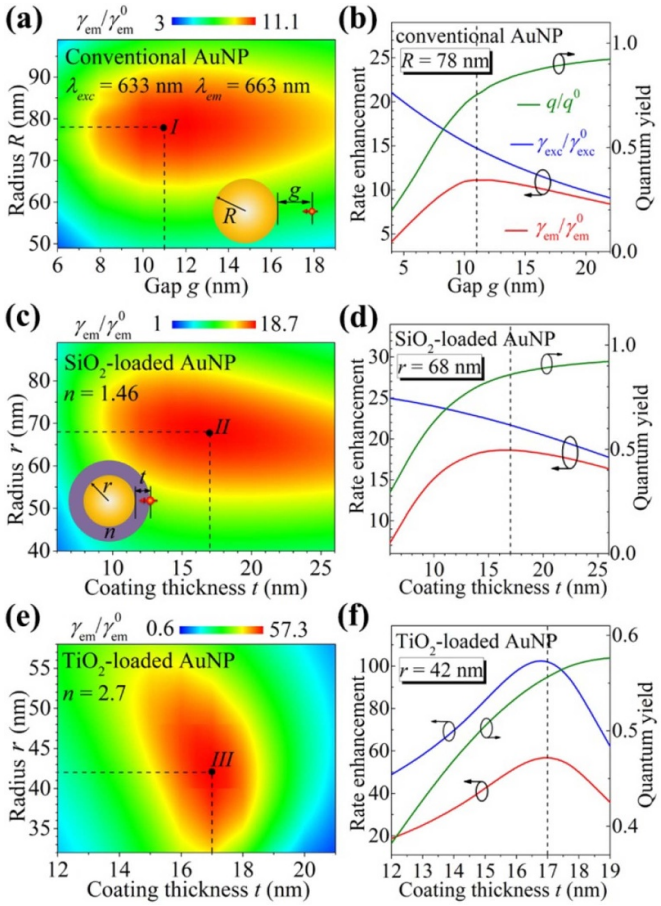


**Figure 4.** (a), (c) and (e) Fluorescence enhancement of a single Nile blue molecule placed near the conventional AuNPs and on the surface of the $SiO_2$-loaded ($n = 1.46$) and $TiO_2$-loaded ($n = 2.7$) AuNPs, respectively. Marked points *I, II* and *III* indicate the maximum fluorescence enhancement. (b), (d) and (f) Normalized quantum yield, excitation rate and fluorescence rate for the conventional AuNPs with $R = 80$ nm, the $SiO_2$-loaded AuNPs with $r = 68$ nm, and the $TiO_2$-loaded AuNPs with $r = 42$ nm as a function of the molecule-Au separation distance, respectively.

the $SiO_2$-loaded AuNPs with $n = 1.46$ and $r = 68$ nm (the intersection point of the vertical dashed line and green curve in figure 4(d)) is thus larger than $f_q \approx 0.79$ achieved in the optimal case of the conventional AuNPs (the intersection point of the vertical dashed line and green curve in figure 4(b)). On the other hand, although the $SiO_2$-loaded AuNPs could not outperform the conventional AuNPs in the maximum achievable field enhancement, the external field enhancement on the outer surface of the $SiO_2$-loaded AuNPs could exceed the field enhancement achieved at a distance away from the conventional AuNPs. The excitation rate of the molecule in the $SiO_2$-loaded AuNPs could reach $f_{exc} \approx 22.1$ at $t = 17$ nm (the intersection point of the vertical dashed line and blue curve in figure 4(d)), which is larger than $f_{exc} \approx 14$ achieved in the conventional AuNPs at $g = 11$ nm (the intersection point of the vertical dashed line and blue curve in figure 4(b)). Compared to the optimal conventional AuNPs, both the excitation rate and the quantum yield are slightly improved in the optimal $SiO_2$-loaded AuNPs, and thus the maximum fluorescence enhancement is correspondingly increased from a factor of ∼11 to ∼19.

For the $TiO_2$-loaded AuNPs, the resonant hot spots could be transferred to the dielectric surface and the maximum field intensity could gain an extra enhancement, as demonstrated in figure 2(a). The molecule coupled to the $TiO_2$-loaded AuNPs is thus expected to sense more intense excitation fields than that in the conventional and $SiO_2$-loaded AuNPs. Unlike the cases of the conventional and $SiO_2$-loaded AuNPs, where the excitation rate enhancement increases monotonically with decreasing the molecule-Au distance (blue curve in figures 4(b) and (d)), the $TiO_2$-loaded AuNPs exhibit a peak in the excitation rate enhancement spectrum (blue curve in figure 4(f)). When the coating thickness of the $TiO_2$-loaded AuNPs with $n = 2.7$ and $r = 42$ nm is tuned to $t = 17$ nm, the excitation rate enhancement could reach a maximum value as high as $f_{exc} \approx 102.8$ (the intersection point of the vertical dashed line and blue curve in figure 4(f)). Compared to the optimal conventional AuNP, the optimal $TiO_2$-loaded AuNP improves the excitation rate by a factor of ∼7, and compared to the optimal $SiO_2$-loaded AuNP, the improvement is almost a factor of ∼5. It is noted that more energy could be transferred from a dipole to the adjacent dielectrics with higher refractive index [41] and also to the nearby metal nanoparticles with smaller size [23]. For this reason, the non-radiative decay rate in the optimal $TiO_2$-loaded AuNP with a relatively higher shell refractive index of $n = 2.7$ and smaller core radius of $r = 42$ nm is expected to be higher than that in the optimal $SiO_2$-loaded AuNP with relatively smaller $n = 1.46$ and larger $r = 68$ nm. The normalized quantum yield in the optimal $TiO_2$-loaded AuNP is found to be $f_q \approx 0.56$ at $t = 17$ nm (the intersection point of the vertical dashed line and green curve in figure 4(f)), which is indeed smaller than $f_q \approx 0.84$ achieved in the optimal $SiO_2$-loaded AuNP at $t = 17$ nm (the intersection point of the vertical dashed line and green curve in figure 4(d)). In spite of the relatively low normalized quantum yield, the resultant fluorescence enhancement in the optimal $TiO_2$-loaded AuNP could reach a maximum value of ∼57, which is improved by a factor of ∼5.2 compared to the optimal conventional AuNP and by a factor of ∼3 compared to the optimal $SiO_2$-loaded AuNP. This reveals that the excitation rate enhancement, which is attributed to the ability of the dielectric-loaded AuNPs to spatially transfer the hot spots and further enhance their intensities, could play a dominant role in the fluorescence enhancement, and thus verifying the importance of the hot-spots engineering provided by the dielectric loading approach.

The extra fluorescence enhancement factors, defined as the ratio of the maximum achievable fluorescence enhancement in the dielectric-loaded AuNPs with different shell materials (i.e. different coating refractive indices) to that in the conventional AuNPs, are also calculated by simultaneously optimizing the core radius $r$ and the coating thickness $t$, and summarized in figure 5. As demonstrated in figure 2(c), the external field enhancement achieved in the dielectric-loaded AuNPs increase monotonically with increasing the coating refractive index, which imposes positive effect on the fluorescence enhancement by increasing the excitation efficiency.

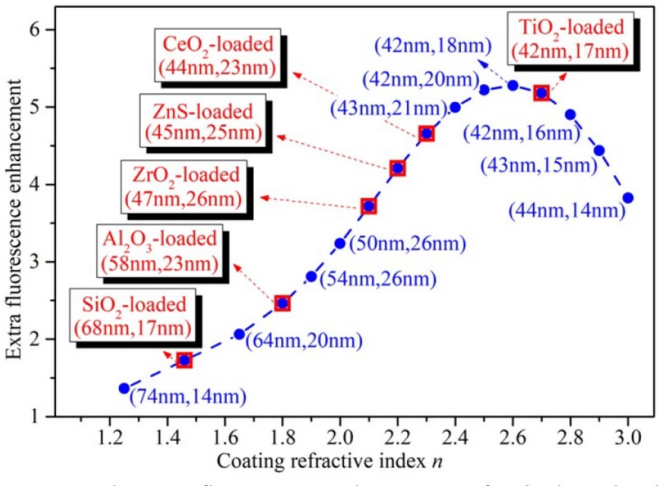


**Figure 5.** The extra fluorescence enhancement of a single molecule coupled to the dielectric-loaded AuNPs with different coating refractive indices. For each coating shell refractive index, the corresponding optimal geometrical parameters are indicated. Hollow squares represent some available coating materials.

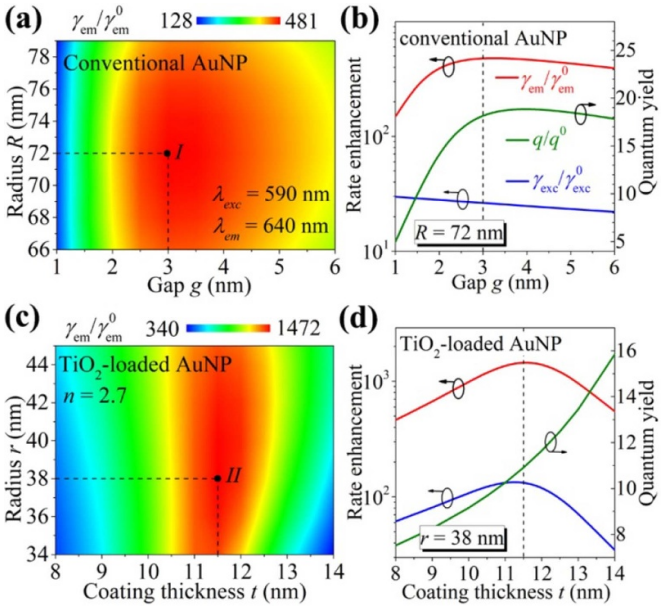


**Figure 6.** (a) and (c) Fluorescence enhancement of a single crystal violet molecule coupled to the conventional and $TiO_2$-loaded ($n = 2.7$) AuNPs, respectively. Marked points *I* and *II* indicate the maximum fluorescence enhancement. (b) and (d) Normalized quantum yield (green), excitation rate (blue) and fluorescence rate (red) for the conventional AuNPs with $R = 72$ nm and the $TiO_2$-loaded AuNPs with $r = 38$ nm as a function of the molecule-Au separation distance, respectively.

Therefore, the extra fluorescence enhancement is found to initially increase with increasing the coating refractive index (figure 5). On the other hand, the optimal core radius is smaller and the corresponding optimal coating thickness is thinner for the dielectric-loaded AuNPs with higher coating refractive index, which could accelerate the non-radiative decay rate [23] and thus impose an adverse effect on the fluorescence enhancement by lowering the quantum yields. As the coating refractive index is increased to $n = 2.6$, the balance is achieved between the increased excitation rate and the decreased quantum yields, and the extra fluorescence enhancement reaches the highest factor of ∼5.3 in the dielectric-loaded AuNPs with optimal core radius of $r = 42$ nm and coating thickness of $t = 18$ nm (figure 5). With further increasing the coating refractive index, the adverse effect of lowering the quantum yields would prevail, and the extra fluorescence enhancement achieved in the dielectric-loaded AuNPs begins to decrease. Nevertheless, within the calculated coating refractive index range from $n = 1.2$ to 3.0, the dielectric-loaded AuNPs could always be optimized to outperform the conventional AuNPs in the fluorescence enhancement.

In the above discussions, a single Nile blue molecule with the peak absorption and emission wavelengths being $\lambda_{exc} = 633$ nm and $\lambda_{em} = 663$ nm is chosen. Here, we also present the fluorescence enhancement results for another type of dye molecule, crystal violet, coupled with the conventional and $TiO_2$-loaded AuNPs. The peak absorption and emission wavelengths of the crystal violet molecules are $\lambda_{exc} = 590$ nm and $\lambda_{em} = 640$ nm, respectively. The intrinsic quantum yield is assumed to be $q^0 = 0.001$. For the single crystal violet molecule coupled with the conventional AuNPs, when the geometrical parameters are optimized to $R = 72$ nm and $g = 3$ nm, the fluorescence enhancement could reach the maximum value of ∼481 (point *I* in figure 6(a)). The detailed energy-transfer rates are also calculated for the conventional AuNPs with $R = 72$ nm and shown in figure 6(b) as a function of the molecule-Au separation distance $g$. It is seen that at the optimal molecule-Au separation distance $g = 3$ nm, in addition to the excitation rate enhancement of $f_{exc} \approx 26.3$, the normalized quantum yield is also significantly enhanced and reaches a factor as high as $f_q \approx 18.3$ (the intersection point of the vertical dashed line and green curve in figure 6(b)), due to the low intrinsic quantum yield of the crystal violet molecule. As a result of both enhancement in the excitation rate and normalized quantum yield, when coupled to the conventional AuNPs, the crystal violet molecules could gain higher fluorescence enhancement than the Nile blue molecules with higher intrinsic quantum yield (figure 6(b) vs figure 4(b)), which is consistent with previously reported results that fluorescence enhancement depends on the intrinsic quantum yield of the molecule and higher enhancement can be achieved for lower $q^0$ [12, 38–40].

Figure 6(c) shows the fluorescence enhancement factors of the single crystal violet molecule coupled to the $TiO_2$-loaded AuNPs with different core radii $r$ and the coating thicknesses $t$. As indicated by the marked point *II*, the maximum fluorescence enhancement is achieved at $r = 38$ nm and $t = 11.5$ nm. By further plotting the energy transfer rates for the $TiO_2$-loaded AuNPs with fixed core radius of $r = 38$ nm as a function of the coating thickness, the excitation rate enhancement is found to reach a peak value of $f_{exc} \approx 135$ at the optimal coating thickness of $t = 11.5$ nm (the intersection point of the vertical dashed line and blue curve in figure 6(d)), and meanwhile the normalized quantum yield reaches an enhancement factor of $f_q \approx 12$ (the intersection

point of the vertical dashed line and green curve in figure 6(d)). Although the normalized quantum yield enhancement in the optimal $TiO_2$-loaded AuNP is slightly smaller than that in the optimal conventional AuNP, the excitation rate in the former case is greatly enhanced (figure 6(d) vs figure 6(b)). Therefore, the fluorescence enhancement achieved in the optimal $TiO_2$-loaded AuNP could reach a maximum value as high as ∼1472. Compared to the optimal case of the conventional AuNPs, the optimal $TiO_2$-loaded AuNP improves the fluorescence enhancement by a factor of ∼3, which demonstrates that the dielectric-loading approach could also be applied to provide an extra enhancement in the fluorescence of the molecules with different transition bands and intrinsic quantum yields.

## 3. Conclusion

In summary, we have demonstrated a dielectric-loading approach for engineering both the intensity and spatial position of the plasmonic hot-spots without the need to change the geometry shape of the well-designed plasmonic nanoantennas. By scaling down the conventional plasmonic nanoantennas and conformally coating them with a high-refractive-index thin dielectric layer, the resultant dielectric-loaded plasmonic nanoantennas could resonate at the same wavelength as the conventional ones, lead to an extra enhancement in the maximum achievable field intensities, and transfer the hot spots from the metal surface to the dielectric surface. We also demonstrate that the shell refractive index plays a key role in the field enhancement, and dielectric-loaded AuNPs with higher shell refractive index could produce larger external field enhancement. When applying on the fluorescence applications, light emitters that are placed on the external surface of the dielectric-loaded plasmonic nanoantennas could sense the transferred and further enhanced hot-spots, which significantly enhance the excitation efficiency of the emitters, and thus improving the fluorescence. Despite demonstrating the significant benefits only on the fluorescence enhancement, the dielectric-loaded plasmonic nanoantennas can be readily designed and optimized for other applications based on the local field enhancement, such as image enhancement, efficient single-photon sources, enhanced nonlinear optical processes, and surface enhanced Raman spectroscopy.

## Acknowledgments

Z C and Z W acknowledge support from the National Key R&D Program of China (2017YFA0303702). Z C and M W acknowledge support from the National Nature Science Foundation of China (11674168, 11774166, 11834007, 11904344 and 11621091). S I B acknowledges support from the University of Southern Denmark (SDU 2020 funding) and the Danish Council for Independent Research (the FTP project PlasTPV, contract no. 1335-00104).

## ORCID iDs

Zhuo Chen https://orcid.org/0000-0002-3246-4171

Ping Gu https://orcid.org/0000-0003-0079-4026

## References

[1] Schuller J A, Barnard E S, Cai W, Jun Y C, White J S and Brongersma M L 2010 *Nat. Mater.* **9** 193
[2] Yu H, Peng Y, Yang Y and Li Z-Y 2019 *Npj Comput. Mater.* **5** 45
[3] Hamann H F, Kuno M, Gallagher A and Nesbitt D J 2001 *J. Chem. Phys.* **114** 8596
[4] Frey H G, Witt S, Felderer K and Guckenberger R 2004 *Phys. Rev. Lett.* **93** 200801
[5] Taminiau T H, Stefani F D, Segerink F B and van Hulst N F 2008 *Nat. Photon.* **2** 234
[6] Moreno E, Rodrigo S G, Bozhevolnyi S I, Martin-Moreno L and Garcìa-Vidal F 2008 *Phys. Rev. Lett.* **100** 023901
[7] Zengin G, Wersall M, Nilsson S, Antosiewicz T J, Kall M and Shegai T 2015 *Phys. Rev. Lett.* **114** 157401
[8] Ruditskiy A and Xia Y 2016 *J. Am. Chem. Soc.* **138** 3161
[9] Liu R, Zhou Z-K, Yu Y-C, Zhang T, Wang H, Liu G, Wei Y, Chen H and Wang X-H 2017 *Phys. Rev. Lett.* **118** 237401
[10] Sundaramurthy A, Crozier K, Kino G, Fromm D, Schuck P and Moerner W 2005 *Phys. Rev.* B **72** 165409
[11] Kim S, Jin J, Kim Y-J, Park I-Y, Kim Y and Kim S-W 2008 *Nature* **453** 757
[12] Kinkhabwala A, Yu Z, Fan S, Avlasevich Y, Müllen K and Moerner W E 2009 *Nat. Photon.* **3** 654
[13] Acuna G P, Möller F M, Holzmeister P, Beater S, Lalkens B and Tinnefeld P 2012 *Science* **338** 506
[14] Russell K J, Liu T-L, Cui S and Hu E L 2012 *Nat. Photon.* **6** 459
[15] Akselrod G M, Argyropoulos C, Hoang T B, Ciracì C, Fang C, Huang J, Smith D R and Mikkelsen M H 2014 *Nat. Photon.* **8** 835
[16] Ciracì C, Hill R T, Mock J J, Urzhumov Y, Fernández-Domínguez A I, Maier S A, Pendry J B, Chilkoti A and Smith D R 2012 *Science* **337** 1072
[17] Esteban R, Borisov A G, Nordlander P and Aizpurua J 2012 *Nat. Commun.* **3** 825
[18] Zhu W and Crozier K B 2014 *Nat. Commun.* **5** 5228
[19] Nie S and Emery S R 1997 *Science* **275** 1102
[20] Dulkeith E, Morteani A C, Niedereichholz T, Klar T A, Feldmann J, Levi S A, van Veggel F C J M, Reinhoudt D N, Möller M and Gittins D I 2002 *Phys. Rev. Lett.* **89** 203002
[21] Gueroui Z and Libchaber A 2004 *Phys. Rev. Lett.* **93** 166108
[22] Ii J T K, Sánchez E J and Xie X S 2005 *Appl. Phys. Lett.* **86** 233102
[23] Anger P, Bharadwaj P and Novotny L 2006 *Phys. Rev. Lett.* **96** 113002
[24] Chen X-W, Agio M and Sandoghdar V 2012 *Phys. Rev. Lett.* **108** 233001
[25] Guerrero A R and Aroca R F 2011 *Angew. Chem., Int. Ed.* **50** 665
[26] Aroca R F, Teo G Y, Mohan H, Guerrero A R, Albella P and Moreno F 2011 *J. Phys. Chem.* C **115** 20419
[27] Osorio-Romań I O, Guerrero A R, Albella P and Aroca R F 2014 *Anal. Chem.* **86** 10246
[28] Camacho S A, Aoki P H B, Albella P, Oliveira O N Jr , Constantino C J L and Aroca R F 2016 *J. Phys. Chem.* C **120** 20530
[29] Johnson P B and Christy R W 1972 *Phys. Rev.* B **6** 4370
[30] Chen H J, Shao L, Li Q and Wang J F 2013 *Chem. Soc. Rev.* **42** 2679

[31] Jackson J D 1999 *Classical Electrodynamics* (Wiley: New York)
[32] Zhang X, Zhao J, Whitney A V, Elam J W and Van Duyne R P 2006 *J. Am. Chem. Soc.* **128** 10304
[33] Tom R T, Nair A S, Singh N, Aslam M, Nagendra C L, Philip R, Vijayamohanan K and Pradeep T 2003 *Langmuir* **19** 3439
[34] Chen H, Shao L, Man Y C, Zhao C, Wang J and Yang B 2012 *Small* **8** 1503
[35] Li B, Gu T, Ming T, Wang J, Wang P, Wang J and Yu J C 2014 *ACS Nano* **8** 8152
[36] Chen T-M, Xu G-Y, Ren H, Zhang H, Tian Z-Q and Li J-F 2019 *Nanoscale Adv.* **1** 4522
[37] Kuhn S, Hakanson U, Rogobete L and Sandoghdar V 2006 *Phys. Rev. Lett.* **97** 017402
[38] Gersten J and Nitzan A 1981 *J. Chem. Phys.* **75** 1139
[39] Bharadwaj P and Novotny L 2007 *Opt. Express* **15** 14266
[40] Meng X, Grote R R, Dadap J I, Panoiu N C and Osgood R M 2014 *Opt. Express* **22** 22018
[41] Catchpole K R and Polman A 2008 *Opt. Express* **16** 21793